Ka-Band Monopulse Antenna-Pointing Systems Analysis and Simulation

V. Y. Lo
Communications Systems and Research Section

NASA's Deep Space Network (DSN) has been using both 70-m and 34-m reflector antennas to communicate with spacecraft at S-band (2.3 GHz) and X-band (8.45 GHz). To improve the quality of telecommunication and to meet future mission requirements, JPL has been developing 34-m Ka-band (32-GHz) beam-waveguide antennas. Presently, antenna pointing operates in either the open-loop mode with blind pointing using navigation predicts or the closed-loop mode with conical scan (conscan). Pointing accuracy under normal conscan operating conditions is in the neighborhood of 5 mdeg. This is acceptable at S- and X-bands, but not enough at Ka-band. Due to the narrow beamwidth at Ka-band, it is important to improve pointing accuracy significantly (∼2 mdeg). Monopulse antenna tracking is one scheme being developed to meet the stringent pointing-accuracy requirement at Ka-band. Other advantages of monopulse tracking include low sensitivity to signal amplitude fluctuations as well as single-pulse processing for acquisition and tracking. This article presents system modeling, signal processing, simulation, and implementation of Ka-band monopulse tracking feed for antennas in NASA/DSN ground stations.

I. Introduction

The design of the DSN monopulse pointing system consists of the reflector antenna, multimode corrugated horn feed, waveguide coupler, monopulse signal processor, and other associated RF electronics. A general block diagram is provided in Fig. 1. Starting at the main reflector, a tapered beam is formed. The HE11 mode in the corrugated horn is excited to radiate the sum pattern while the TE21 mode waveguide coupler generates the difference pattern [1]. With the assumption of perfect Ka-band-to-IF conversion, signal processing starts in the IF domain. A phase-locked loop recovers the carrier phase. This is used as a phase reference to coherently demodulate the elevation and azimuth difference channels. The sum and difference baseband signals are low-pass filtered and then followed by monopulse signal processing from which elevation and azimuth pointing errors are estimated. The error signals are used to drive the antenna servo controller for pointing corrections.

To predict the overall system performance, an antenna system model is needed. Mathematical models of the open-loop S-curve and pointing variance are presented in Section II. These models are validated by comparison with the difference pattern generated by a single-aperture multimode antenna. In Section III, a simplified servo loop model on the antenna controller and driver system is described. Higher-order complex multistate models are reserved for future upgrade. An end-to-end DSN block simulation

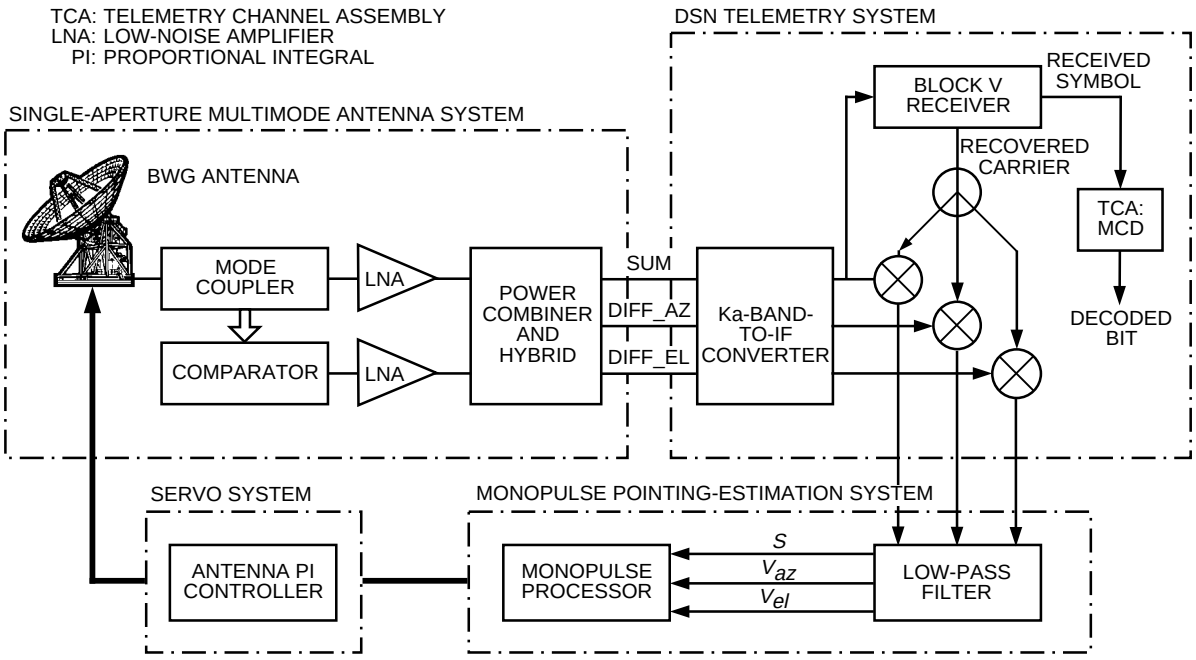

Fig. 1. Antenna-pointing system with monopulse signal processing.

program is presented in Section IV. The system includes the monopulse antenna block for a single-aperture multimode antenna, the digital receiver block for the Block V receiver (BVR), the decoder block for the maximum-likelihood convolutional decoder (MCD), the low-pass filter (LPF) and the monopulse processor blocks for pointing-error estimation, and the servo block for the antenna driver controller. Finally, in Section V, open- and closed-loop system performance in the presence of noise, cross-channel interference, amplitude and phase imbalance, and wind loading are investigated using this block simulation program.

II. System Model of Monopulse Antenna Pointing

Based on the physics of a corrugated horn and mode coupler, the classical four-horn monopulse antenna is shown to produce the same open-loop S-curve as the monopulse single-aperture multimode antenna.[1] In the presence of random noise, it can also be shown that the carrier-to-noise power spectral density ratio (CNR) is identical between the four-horn model and the single-aperture model with the same aperture size. Thus, the four-horn model produces the same system performance as a single-aperture multimode antenna under identical input signal conditions. The simple four-horn model can now be used for system simulation and analysis. Without loss of generality, we shall examine the azimuth pointing errors only.

From a complex signal analysis on a four-horn model [2,3],[2] the mean error voltage and its variance are shown to be

[1] S-curves from various models were compared under deterministic conditions in T. K. Wu, "Monopulse Antenna Study," JPL Interoffice Memorandum 3365-94-MP-001 (internal document), Jet Propulsion Laboratory, Pasadena, California, September 1994, and in V. Lo, "Single Aperture Multi-Mode Monopulse Antenna Pointing With Corrugated Horn," JPL Interoffice Memorandum 3393-94-VYL-015 (internal document), Jet Propulsion Laboratory, Pasadena, California, November 1994.

[2] The detailed mathematical derivation is shown in V. Y. Lo, "Monopulse Tracking Feed Link Study," JPL Interoffice Memorandum 339-92-134 (internal document), Jet Propulsion Laboratory, Pasadena, California, December 1992.

$$v_{az} = \frac{1}{2}\tan\left[\frac{\pi}{\lambda}d\sin\left(\theta_{az}\right)\right]\left[1+\cos\left(\frac{2\pi}{\lambda}d\sin\left(\theta_{el}\right)\right)\right] \tag{1a}$$

$$\sigma_v^2 = \left|\frac{\delta_{az}}{S}\right|^2 \frac{1}{SNR_s} + \frac{1}{SNR_{az}} - 2\left|\frac{\delta_{az}}{S}\right| \frac{1}{SNR_{az}} \tag{1b}$$

where

$v_{az}, \sigma_v^2 =$ the mean error voltage and its variance

$\theta_{az}, \theta_{el} =$ the azimuth and elevation pointing errors

$\delta_{az} =$ the azimuth difference signal

$d =$ the distance between adjacent horns

$|S|^2 =$ the signal power

$SNR_S = \dfrac{|S|^2}{\sigma_s^2} =$ the sum channel SNR

$SNR_{az} = \dfrac{|S|^2}{\sigma_{az}^2} =$ the azimuth channel carrier SNR

$SNR_c = \dfrac{|S|^2}{\rho\sigma_s\sigma_{az}} =$ the cross-channel SNR

$\rho =$ the correlation coefficient between the sum and azimuth channels

$\sigma_s^2, \sigma_{az}^2 =$ the variance of the sum and azimuth channels

For a high CNR and a small pointing error, the pointing error and its variance simplify to

$$\theta_{az} = \frac{v\lambda}{\pi d} \tag{2a}$$

$$\sigma_\theta^2 = \left(\frac{\lambda}{\pi d}\right)^2 \left(\frac{1}{SNR_{az}}\right) \tag{2b}$$

The 34-m Ka-band beam-waveguide (BWG) antenna parameters can now be substituted into Eqs. (1) and (2). For $d/\lambda = 1000$, the pointing-error voltage plot from Eq. (1a) is compared with S-curves generated from other physics and SPW [3] simulation models in Fig. 2. It shows that, at medium pointing errors, the mathematical model from Eq. (1a) matches the physics model of a single-aperture multimode antenna as well as the SPW-simulated S-curve of a four-horn monopulse antenna. Since a monopulse processor essentially performs integration on the input signal CNR to optimized pointing-error estimates, Eq. (2b) can be rewritten in terms of integration time T, $\sigma_\theta = (18\times10^{-3})\left[1/\sqrt{(CNR\cdot T)}\right]$. The linearized standard deviation is plotted against the integration time for CNR values ranging from 10 to 30 dB-Hz

[3] Signal Processing WorkSystem (SPW) is the registered trademark of Alta Group, formerly Comdisco Systems, Inc.

(see Fig. 3). Based on the DSS-13 KABLE [4] link prediction, the carrier-to-noise power spectral-density ratio is expected to be greater than 10 dB-Hz. For a CNR value of 10 dB-Hz and a pointing error of 2 mdeg, integration time is 8 s. Given the possible range of CNR, 0.08 to 8 s represents the corresponding spread in integration time. For stable loop operation, the observation time of the estimator has to be short compared to the update time of the servo loop.

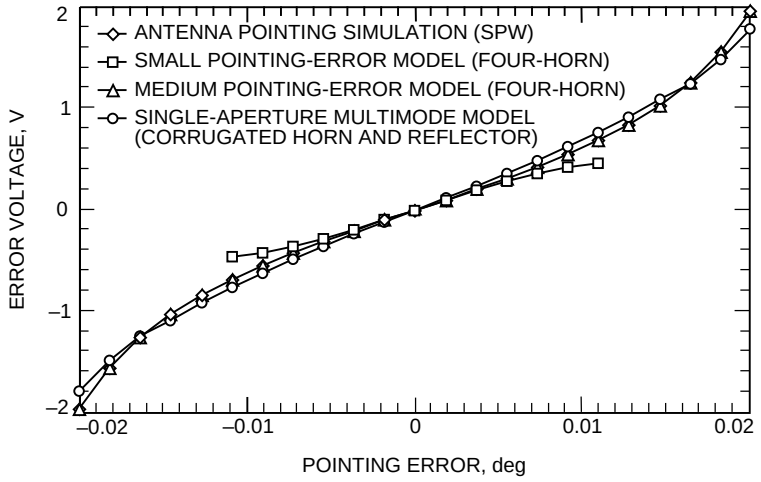

Fig. 2. Comparison of simulation, small/medium pointing-error models, and the single-aperture multimode model.

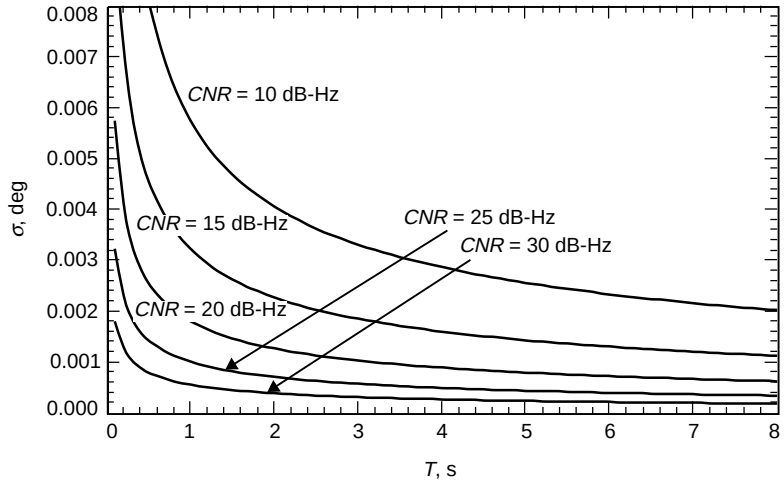

Fig. 3. Standard deviation of pointing error from the linearized model.

III. Simplified Servo Loop Model of the DSN Ground Antenna

A model of the DSN BWG antenna servo control system [4] based on DSS 13 was developed to study pointing dynamics, channel cross-coupled dynamics, and wind disturbances. The state–space model of the antenna structure was obtained from its finite-element model. State reduction was applied separately on the antenna structure, elevation and azimuth drives, and rate-loop model. To a first-order approximation,

[4] The Ka-band link experiment (KABLE) was presented in *OSC Advanced Systems Review: TDA Systems Development* (internal document), Jet Propulsion Laboratory, Pasadena, California, June 1992.

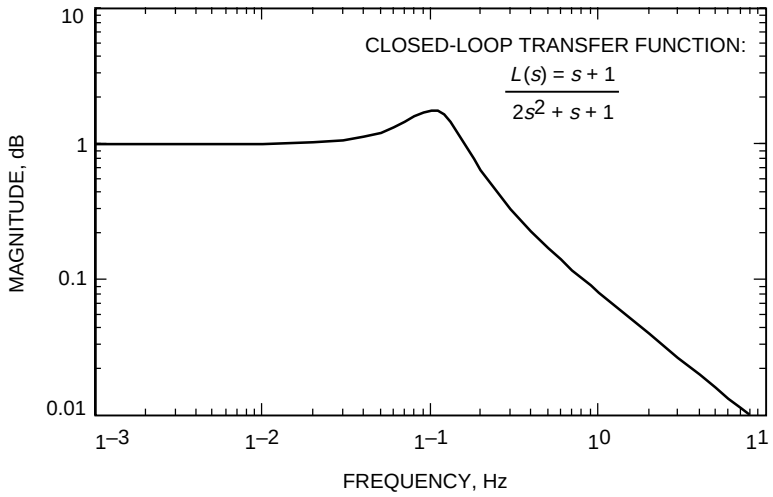

Fig. 4. Magnitude response of the servo loop model.

a proportional controller is used as a pointing-error estimator based on the observed differential error voltages. Such information is passed on to the elevation and azimuth drives to turn the antenna structure. This second-order servo loop model is shown in Fig. 4. The frequency response has a 3-dB roll-off at 0.2 Hz.

IV. End-to-End DSN Ground-Link Simulation

APSIM_MON is a simulation software [5] of the DSN BWG antenna supporting the Ka-band monopulse development effort. It is constructed on the platform of the SPW. The hierarchy simulation model for monopulse antenna pointing (ANT_MON) has been integrated with the advanced digital receiver model (DIG_RCVR) and the decoder model (CON_DEC) to form an end-to-end DSN telemetry system (see Fig. 5).[5] The proper encoded signal is available through the simulation signal generator (CC_SIG) model, which generates an encoded pseudonoise (PN) data sequence with different initial phase and frequency conditions. Parameters of the SNR, loop acquisition, and running averages of the bit error rate are monitored by the simulation monitor block (PERF_MONITOR).

The simulation model has been applied to analyze various design parameters. The following cases have specifically been investigated:

(1) Open-loop monopulse antenna pointing with and without random noise

(2) Closed-loop monopulse antenna pointing with and without random noise

(3) Effects of amplitude and phase imbalance between the sum and difference channels

(4) Effects of pointing errors on end-to-end telemetry link performance

[5] The SPW Costas-loop digital receiver model developed by J. Gevargiz for the BVR has been expanded to include residue carrier with square- and sine-wave subcarriers; see J. Gevargiz, "Acquisition, Tracking and Bit-Error-Rate Analysis of the Block V Receiver's BPSK Tracking Loop Including the Convolutional Coder and Decoder," JPL Interoffice Memorandum 3396-93-05 (internal document), Jet Propulsion Laboratory, Pasadena, California, March 1993, and V. Lo, "Antenna Pointing Simulation With Monopulse Processing (APSIM_MON)," JPL Interoffice Memorandum 3393-95-VYL-02 (internal document), Jet Propulsion Laboratory, Pasadena, California, April 1995.

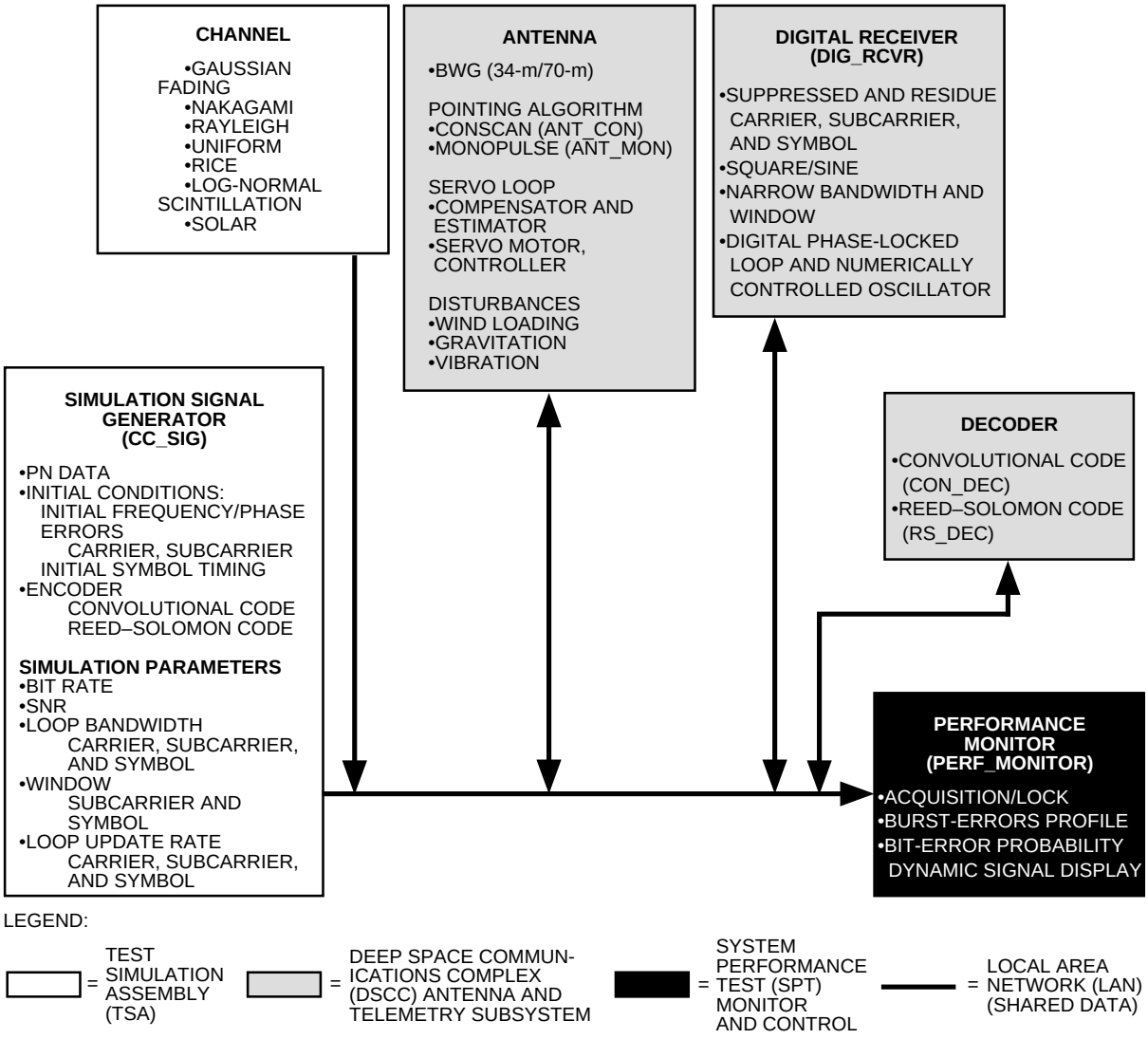

Fig. 5. SPW simulation of the monopulse antenna-pointing system.

V. Summary of Simulation Results

For case (1), with variable pointing errors, the corresponding error voltages in the forward loop trace out the S-curve shown in Fig. 2. When Gaussian noise is added into the loop, a noisy pointing-error voltage is observed. The standard deviation of the linearized mathematical prediction based on the corrupt pointing-error voltage, Eq. (2), is shown in Fig. 3. Knowing the input SNR, these curves provide the integration time needed to meet a specific pointing-error variance.

For case (2), a simple second-order servo loop is used to model the antenna controller. The frequency response has a 3-dB roll-off at 0.2 Hz (see Fig. 4). Stability of the servo loop is investigated as a function of the low-pass filter bandwidths in the forward path. Various types of low-pass filters, including Butterworth, Bessel, and Chebyshev, with up to twenty orders are used in this evaluation. Deterministic step responses of the loop are simulated (see Fig. 6). The results show that the low-pass filter bandwidth has to be about two orders of magnitude higher than the servo-loop bandwidth for stable loop operations.

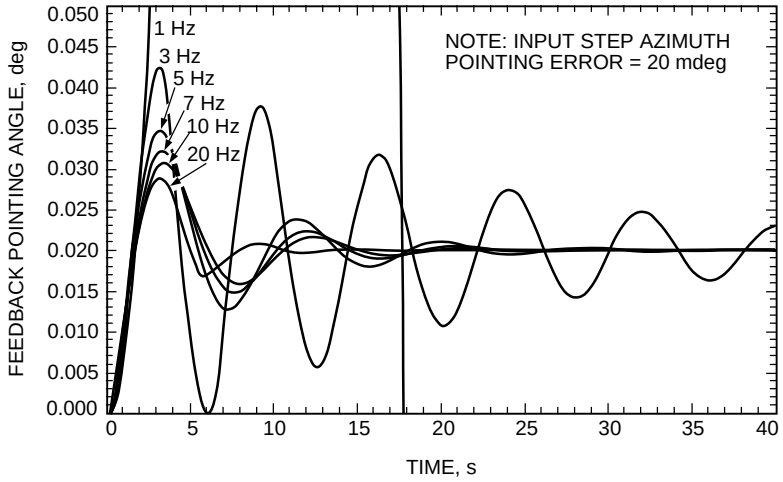

Fig. 6. Simulated closed-loop step response as a function of LPF bandwidth.

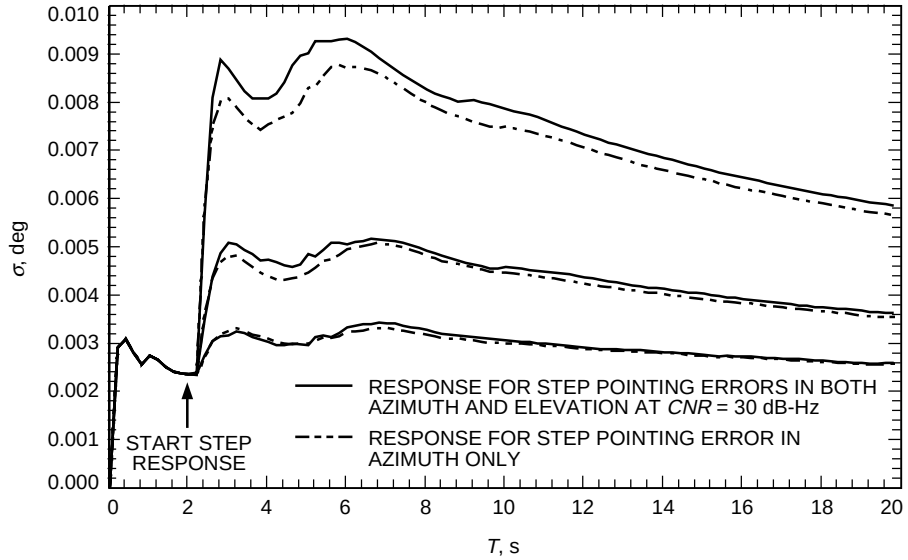

Fig. 7. Standard deviation of closed-loop pointing error of the azimuth channel induced by step perturbation in single and dual channels.

The same conclusion can also be reached from root locus and Nyquist stability analyses. In the presence of uncorrelated Gaussian noise, the simulated standard deviations of closed-loop step pointing error for single-channel and cross-channel interference are shown in Fig. 7. Coupling between the azimuth and elevation channels will increase the pointing error beyond this baseline.

For case (3), the amplitude imbalance between the sum and difference channels scales the voltage of the S-curve while the relative phase imbalance in electrical length manifests as a bias of the pointing error. The source of such imbalance may be due to amplifiers, hybrids, couplers, filters, etc. Both open- and closed-loop pointing-error variances are also modified by a multiplication factor of the squared amplitude imbalance. These results are summarized in Fig. 8, where a relative amplitude of 1 and a relative phase of 0 deg represent the baseline with no imbalance. Offsets corresponding to 0.1- and 1-dB pointing losses are marked by dotted lines in the figure for reference. Specifications on amplitude and phase mismatch between the difference and sum channels can now be established to meet pointing-loss tolerance.

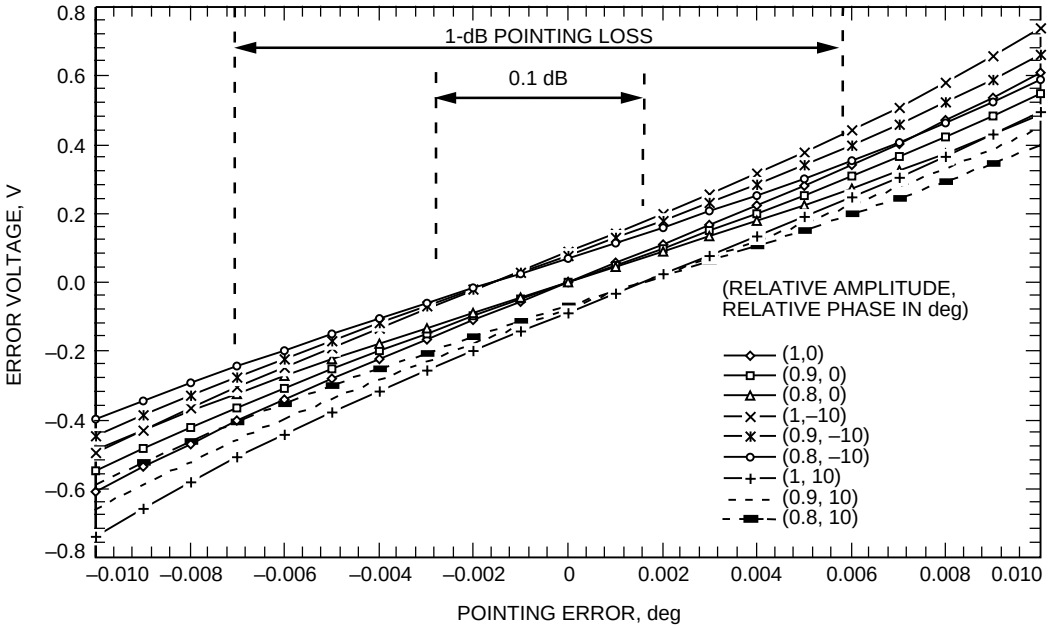

Fig. 8. Effects of cross-channel amplitude and phase distortion on the S-curve.

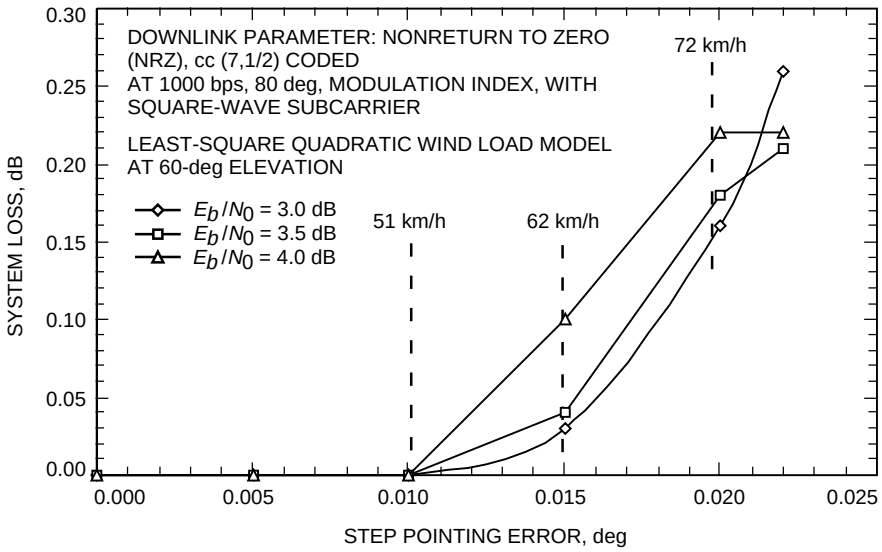

Fig. 9. System loss due to step pointing error.

Finally, the impact of pointing errors on the link quality driven by wind loading or gravitational effects can now be analyzed by observing the relative increase in bit errors after the onset of such disturbances. The loss in signal power relative to the unperturbed case can be obtained from the increase in bit-error probability. For example, a 1-kbps downlink with a (7,1/2) convolutional code at an 80-deg modulation index in a monopulse closed-loop pointing system with system loss from step pointing error induced by wind load is shown in Fig. 9. Unlike the antenna pointing loss from miscalibration, this peak pointing loss represents a dynamic process depending on the rate of change of the disturbance relative to the servo loop tracking rate. Similar to radio loss in carrier tracking, the results show that the telemetry link is more susceptible to small pointing errors at high SNR.

VI. Conclusion

A system model for monopulse antenna pointing has been presented. Under the framework of SPW simulation, a monopulse antenna block is constructed from this system model. Both open- and closed-loop responses in the presence of noise are investigated through simulation. Pointing performance is evaluated from the perspective of SNR degradation (system loss) on an end-to-end link due to wind loading. These simulation results provide the basis for design, implementation, and performance evaluation of the DSN Ka-band monopulse pointing system.

Acknowledgments

I would like to acknowledge the technical support by M. K. Sue and T. K. Wu.

References

[1] P. J. Clarricoats and A. D. Olver, *Corrugated Horns for Microwave Antennas*, London: Peter Peregrinus Ltd., 1984.

[2] T. Inoue and T. Kaitsuka, "K-Band Tracking System for Domestic Satellite Communication System," *IEEE Trans. on Aerospace and Electronic Systems*, vol. AES-17, no. 4, pp. 561–570, July 1981.

[3] S. Sharenson, "Angle Estimation Accuracy With a Monopulse Radar in the Search Mode," *IRE Trans. on Aerospace and Navigation Electronics*, vol. ANE9, no. 3, pp. 175–179, September 1962.

[4] W. Gawronski and J. A. Mellstrom, "Modeling and Simulations of the DSS 13 Antenna Control System," *The Telecommunications and Data Acquisition Progress Report 42-106, April–June 1991*, Jet Propulsion Laboratory, Pasadena, California, pp. 205–248, August 15, 1991.

[5] V. Y. Lo and M. K. Sue, "Monopulse Signal Processing and Simulation for DSN Beam Waveguide Antenna," *Proc. ICSPAT*, vol. 2, Boston, Massachusetts, pp. 1603–1607, October 1995.